Electronic Supplementary Information (ESI) for

Do equilibrium and rate constants of intramicellar reactions depend on micelle size ?

By Tim Kohlmann and Martin Goez[*]

Contents

[*]Tim Kohlmann, Prof. Dr. Martin Goez,
Martin-Luther-Universität Halle-Wittenberg, Institut für Chemie, Kurt-Mothes-Str. 2, D-06120 Halle (Saale), Germany.
E-mail: martin.goez@chemie.uni-halle.de

1 Experimental Details

Most of the chemicals were pure enough as received (pyrene, $>$ 99 %, Fluka; methyl viologen dichloride, 98 %, Sigma-Aldrich; sodium chloride, $\geq$ 99.5 %, Sigma-Aldrich; methanol, spectrophotometric grade, $\geq$ 99.9 %, Sigma-Aldrich; sodium nonyl, decyl and tridecyl sulfate, all 99 %, Alfa Aesar; sodium undecyl sulfate, 99 %, SCBT; sodium dodecyl sulfate, $>$ 99.5 %, Roth). The only exception was sodium tetradecyl sulfate (95 %, Sigma-Aldrich), which we purified by recrystallization from ethanol.

The alkyl sulfates were dried prior to use; in the case of the quencher methyl viologen MV^{2+}, we instead determined the water content (about 15 % according to our thermogravimetric analysis) and took it into account when calculating the weight-in concentrations. For each experimental series, we freshly prepared the samples with ultrapure Millipore Milli-Q water (specific resistance, 18.2 MΩ cm^{-1}), deoxygenated them with argon (purity 5.0, AirLiquide), and performed the measurements on them within a few hours to minimize the risk of hydrolysis. The experiments in methanol followed the analogous protocol.

Steady-state absorption, steady-state luminescence, and time-resolved luminescence were recorded with a Shimadzu UV-1800 spectrophotometer, a Perkin-Elmer LS 50B fluorescence spectrometer, and an Edinburgh Instruments FS5 time-correlated single-photon counting apparatus (excitation source, EPLED-340; 341 nm, FWHM 7.8 nm and 0.8 ns); all three were equipped with thermostated cell holders. In the luminescence experiments, the samples were optically thin at the excitation wavelength (10 μM pyrene, corresponding to an optical density of about 0.4; MV^{2+} nonabsorbing) and completely transparent at the detection wavelength (395 nm).

None of the termination criteria of time-correlated single-photon counting — number of counts in the maximum channel or in total; alternatively, total acquisition time — result in an absolute vertical scaling that would allow amplitude comparisons between different experiments. However, a meaningful analysis of static quenching hinges on such comparisons. On each sample and at the same temperature, we therefore recorded both the luminescence decay and the stationary luminescence. Using numerical integration (i.e., summation over all the channels), we then rescaled the former with the aid of the latter. This straightforward normalization procedure only demands complete decay of the pyrene fluorescence between excitations in the time-resolved experiment, which we ensured by setting the interpulse delay to 5 μs, i.e., longer than ten times the unquenched fluorescence lifetime.

2 Data Analysis

To keep this section self-contained, we have duplicated two equations and two figures of the main article herein. We refer to the methyl viologen as MV^{2+} only when its specific properties are concerned, and as Q whenever its function as quencher occupies the foreground.

Supplementary Table 1 juxtaposes the functions describing combined static and dynamic quenching in homogeneous medium and in micellar solution without solubilizate exchange. Whereas the former are textbook knowledge, the latter have recently been derived by us through a kinetic approach.[1] Our closed-form expressions are mathematically equivalent to earlier results, which were obtained by Gehlen and DeSchryver through a stochastic treatment and partly specified as infinite series;[2] and Supplementary Equation S2a turns into the Infelta–Tachiya equation[3,4] when there is no static quenching.

Supplementary Table 1: Functions for the time-resolved luminescence decays (TR) and Stern–Volmer experiments (SV) with combined static and dynamic quenching; equation numbers in boxes to the right of the pertaining formulas.

Observable[a]		Homogeneous solution[b]		Micellar environment[b,c,d]	
TR:	$\frac{f(t)}{f_0}$	$\frac{\exp\left[-k\,[\mathrm{Q_t}]\,t\right]\,\exp\left[-t/\tau\right]}{1+K\,[\mathrm{Q_t}]}$	S1a	$\frac{\exp\left[-\langle q\rangle\left(1-\exp\left[-k_\mathrm{m}t\right]\right)\right]\,\exp\left[-t/\tau\right]}{1+K_\mathrm{m}\langle q\rangle}$	S2a
SV:	$\frac{F_0}{F}$	$\left(1+K\,[\mathrm{Q_t}]\right)\left(1+k\tau\,[\mathrm{Q_t}]\right)$	S1b	$\left(1+K_\mathrm{m}\langle q\rangle\right)\frac{k_\mathrm{m}\tau\,\exp\left[+\langle q\rangle\right]}{\left(-\langle q\rangle\right)^{-1/(k_\mathrm{m}\tau)}\,\gamma\left[1/(k_\mathrm{m}\tau),\,-\langle q\rangle\right]}$	S2b

[a] f_0 and F_0, initial luminescence and stationary luminescence without quencher but with all other conditions identical. [b] Common parameters: k, quenching rate constant; $[\mathrm{Q_t}]$, quencher weight-in concentration; τ, lifetime of the excited probe (fluorophore) without quenching in the homogeneous case, or without intramicellar quenching in the micellar case; K, equilibrium constant for formation of a ground-state complex between probe and quencher. [c] Derived parameters: $\langle q\rangle$, micellar occupation (Supplementary Equation S4); k_m and K_m, k and K divided by the molar micellar volume V_m. [d] Special function: $\gamma\,[a,\,z]$, lower incomplete Gamma function (Supplementary Equation S9).

The expressions in Supplementary Table 1 have been rearranged such as to emphasize their similarities in the two media. It is seen that the static quenching in all cases, and the natural decay of the fluorophore in the time-resolved cases, merely contribute multiplicative factors, which can thus be separated from the functions describing the dynamic quenching. Moreover, the static quenching terms have identical forms except for a replacement of $K\,[\mathrm{Q_t}]$ by $K_\mathrm{m}\langle q\rangle$ in the microheterogeneous medium, which arises because the treatment of intramicellar reactions is based on occupation numbers rather than concentrations.

The mean micellar occupation $\langle q\rangle$ with quencher molecules is frequently estimated with Supplementary Equation S3,

$$\langle q\rangle \quad = \quad N_\mathrm{agg}\times\frac{[\mathrm{Q_t}]}{[\mathrm{Surf_t}]-\mathrm{cmc}} \tag{S3}$$

on the basis of the weight-in concentrations $[\mathrm{Q_t}]$ and $[\mathrm{Surf_t}]$ of the quencher Q and the surfactant Surf, as well as the aggregation number N_agg and the critical micelle concentration cmc as parameters of Surf. The correct expression for $\langle q\rangle$ is, however, given by Supplementary Equation S4,

$$\langle q\rangle \quad = \quad N_\mathrm{agg}\times\frac{[\mathrm{Q_m}]}{[\mathrm{Surf_m}]} \tag{S4}$$

which uses the concentrations $[\mathrm{Q_m}]$ and $[\mathrm{Surf_m}]$ of Q and Surf that are actually solubilized and

in the aggregated state, respectively. Their determination is described below, in Sections 3.1 and 3.3.

The parameters K_m and k_m are defined for one quencher molecule in one micelle. Hence, K_m is dimensionless and k_m is a first-order rate constant; and a multiplication with the molar micellar volume V_m transforms both parameters such that they have the usual units of quenching in homogeneous solution.

Supplementary Figure 1 serves to explain our protocol for parameter extraction from the measurements, with Supplementary Figure 1a displaying the raw data after scaling the time-resolved traces with the aid of the Stern–Volmer data, as described in Section 1. We stress that no fits to any model function are needed for this step. After its completion, the Stern–Volmer results are no longer needed, but have been included for completeness.

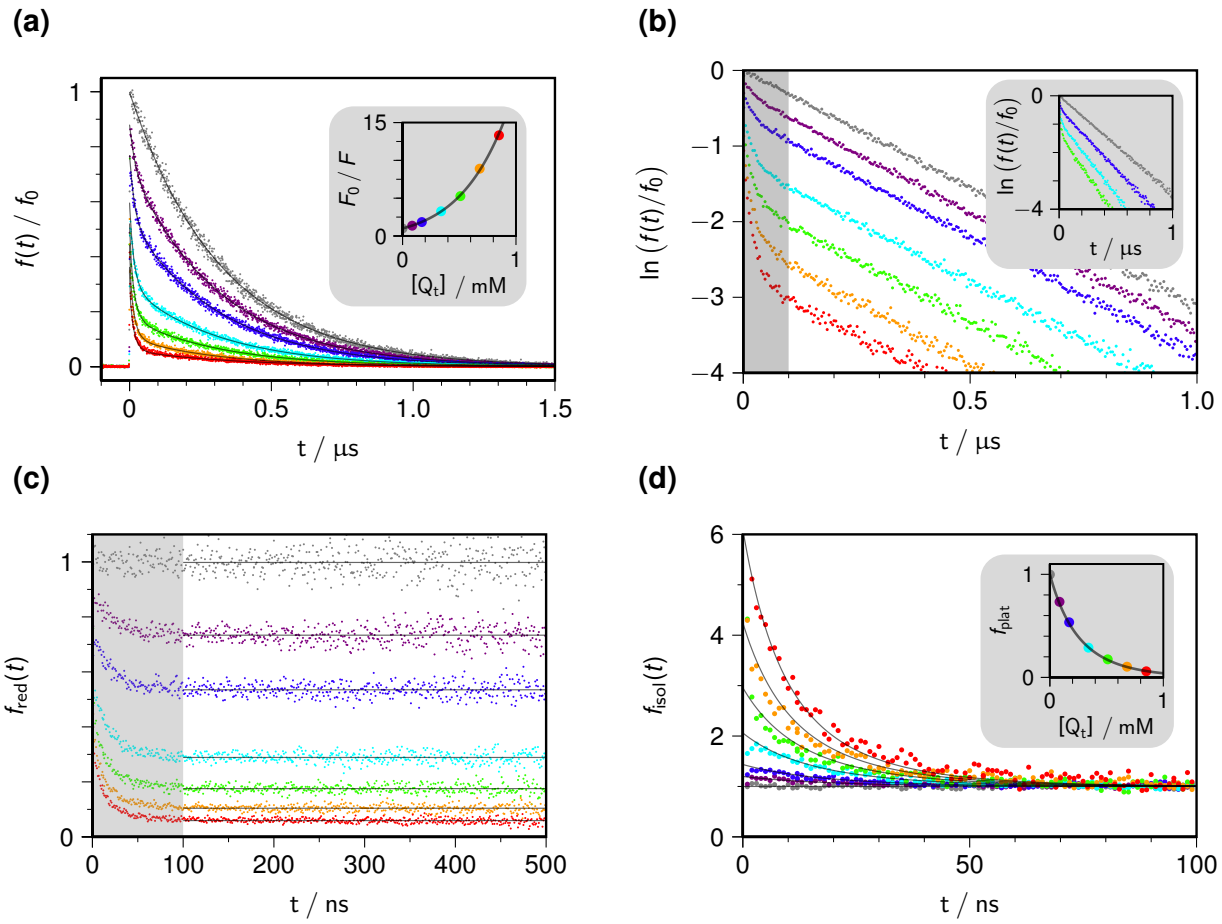

Supplementary Figure 1: Illustrating the data analysis and the fit procedure for the combined intramicellar quenching; same colour code for [Q_t] throughout. Graphs (a) and (b) are identical to Figures 1a and 1b of the main article; all experimental parameters and fit results can also be found there. Graph (c): reduced curves $f_{red}(t)$, obtained by multiplication of the original decay traces with $\exp[+t/\tau]$. Graph (d): plateau values f_{plat} and isolated decays $f_{isol}(t)$ (inset and main plot), fit functions given by Supplementary Equations S7 and S8. For further explanation, see the text.

The multiplicative term $\exp\left[-t/\tau\right]$ in the numerator of Supplementary Equation S2a describes the contribution of micelles hosting an excited fluorophore but no quencher. It manifests itself as a straight line in a log-lin plot of $f(t)/f_0$ after the much faster intra-

micellar processes are completed (at times longer than about 100 ns in the main plot of Supplementary Figure 1b, and considerably earlier in the inset).

If there is no quenching through the micellar interface, τ does not depend on the quencher concentration and equals the natural radiative lifetime τ_0; hence the lines for different $[Q_t]$ are strictly parallel to one another. This evidently holds true for the main plot of Supplementary Figure 1b. The inset of that Supplementary Figure serves as a counterexample: there, slow quenching through the micellar interface (rate constant, k_{ext}) plays a role because a substantial fraction of Q has been displaced from the micellar surfaces into the aqueous phase by the addition of sodium ions in high concentration. Quenching of the solubilized fluorophore through the micelle-water interface is a (pseudo) first-order reaction without a static quenching component.

Supplementary Equation S5 takes into account the lifetime shortening through this process,

$$\frac{1}{\tau} \quad = \quad \frac{1}{\tau_0} + k_{ext} \left[Q_{aq}\right] \quad = \quad 1/\tau_0 + k_{ext}\, r\, [Q_t] \tag{S5}$$

and Supplementary Equation S6 provides the connection between the quencher concentrations in the aqueous phase, in micellized form, and in total,

$$r \quad = \quad \frac{\left[Q_{aq}\right]}{[Q_t]} \quad = \quad 1 - \frac{[Q_m]}{[Q_t]} \tag{S6}$$

With increasing $[Q_t]$, but under otherwise identical conditions, the slopes in the log-lin plot thus become steeper, which is clearly seen in the inset of Supplementary Figure 1b and allows extracting the rate constant k_{ext} of that quenching variant in a straightforward way, with Supplementary Equations S5 and S6.

We point out that our derivation of the equation for the fluorescence decays, Supplementary Equation S2a, hinges on the intramicellar quenching being significantly faster than (i) quenching through the interface, and (ii) exit of the quencher from the micelles. The first criterion is met in our systems, as can be concluded from the log-lin plots, which invariably showed that conditions favourable for the latter process are accompanied by a significant acceleration of the former process (as an example, see the inset of Supplementary Figure 1b, where the nonlinear regime is almost too short to be discernible). Given these data, the second requirement is also fulfilled, as follows from the estimations of the exit rates in Section 3.2.

Our fit procedure is essentially free from problems with parameter uniqueness and utilizes two transformations. First, we multiply each decay with $\exp\left[+t/\tau\right]$, where the parameter τ is obtained by a single-parameter fit over the monoexponential range, whose starting point can be immediately read off from Supplementary Figure 1b. From inspections of these plots, it is evident that the required back extrapolation (over an time not larger than 10–20 % of the fit interval) does not compromise reliability.

This transformation blanks out the natural decay including the quenching through the micellar interface, when present. Supplementary Figure 1c collects the resulting set of reduced decays $f_{\mathrm{red}}(t)$. These are seen to become horizonal in the "late" regime, as they must, with plateau values f_{plat} given by Supplementary Equation S7,

$$f_{\mathrm{plat}} \quad = \quad \lim_{t\to\infty} f_{\mathrm{red}}(t) \quad = \quad \frac{\exp\left[-\langle q\rangle\right]}{1 + K_{\mathrm{m}}\langle q\rangle} \tag{S7}$$

and displayed as function of $[\mathrm{Q_t}]$ in the inset of Supplementary Figure 1d.

Because $[\mathrm{Q_m}]$ — if it deviates at all from $[\mathrm{Q_t}]$ — can be determined independently (Section 3.1), the aggregation number N_{agg} is the one micellar parameter to be adjusted, that is, to be extracted from the constant of proportionality between $[\mathrm{Q_m}]$ and $\langle q\rangle$. In the absence of static quenching, the denominator of Supplementary Equation S7 would become unity, and another single-parameter fit would immediately yield N_{agg}. When there is static quenching, however, a cross correlation of the two fit parameters N_{agg} and K_{m} cannot be excluded because the curve shape is not very distinct.

The remedy is provided by a second transformation, namely, division of $f_{\mathrm{red}}(t)$ by f_{plat} to give the isolated decays $f_{\mathrm{isol}}(t)$, of Supplementary Equation S8

$$f_{\mathrm{isol}}(t) \quad = \quad \exp\left[\langle q\rangle \exp[-k_{\mathrm{m}}t]\right] \tag{S8}$$

which are shown in the main plot of Supplementary Figure 1d. This transformation removes the parameter K_{m}; the amplitude of $f_{\mathrm{isol}}(t)$ responds only to N_{agg}, hence this fit parameter is decoupled from the other one, k_{m}; and re-inserting N_{agg} thus obtained into Supplementary Equation S7 finally allows a single-parameter fit for the determination of K_{m}.

A further great impovement of parameter uniqueness and significance finally comes from a global fit of a series of time-resolved experiments with varying $[\mathrm{Q_t}]$ under otherwise identical conditions. Within such a set, the quantities N_{agg}, K_{m} and k_{m} must remain the same; potential changes of τ are removed individually by the first transformation; and the constant of proportionality relating $\langle q\rangle$ and $[\mathrm{Q_t}]$ cannot change under these circumstances. Supplementary Figure 1a demonstrates that the global three-parameter basis of N_{agg}, K_{m} and k_{m}, with τ reinserted from the local fit, perfectly accommodates all six curves recorded with nonzero quencher concentrations spanning an order of magnitude.

As we recently derived,[1] combined static and dynamic intramicellar quenching causes the Stern–Volmer observable F_0/F to follow Supplementary Equation S2b, which involves the lower incomplete Gamma function (Supplementary Equation S9),

$$\gamma(a,z) \quad = \quad \int_0^z \zeta^{a-1}\exp(-\zeta)\,\mathrm{d}\zeta \tag{S9}$$

This function yields complex values for negative z and positive a, but the combination with z^{-a}, in which it appears in Supplementary Equation S2b, ensures a real-valued product. All

major programming languages contain efficient implementations of $\gamma(a, z)$ in their libraries.[5]

The inset of Supplementary Figure 1a shows that the theoretical Stern–Volmer curve (Supplementary Equation S2b) calculated with the parameters obtained from the time-resolved measurements is in perfect agreement with the experimental Stern–Volmer results. This is hardly surprising: it is self-evident that a parameter set that describes the decays so well must also reproduce their integrals, hence the corresponding Stern–Volmer curve, equally well. However, a reversal of this argument would be fallacious: the values extracted from a Stern–Volmer curve by fitting Supplementary Equation S2b with four parameters, one of which (namely, τ) might even be different for each quencher concentration, will in most cases be meaningless on account of strong interparameter correlations; and the interpretational danger lies in the fact that such a fit will generally look deceptively good.

3 Auxiliary Experiments and Calculations

3.1 Separation of Free and Micelle-bound MV^{2+}

As is evident from the log-lin plots (compare, the inset of Supplementary Figure 1b), the addition of NaCl, especially at elevated temperatures, leads to a displacement of MV^{2+} from the micellar surface into the aqueous bulk to some degree. To determine the partitioning between the locations, we recorded absorption spectra of MV^{2+} under different conditions. Supplementary Figure 2 presents an example.

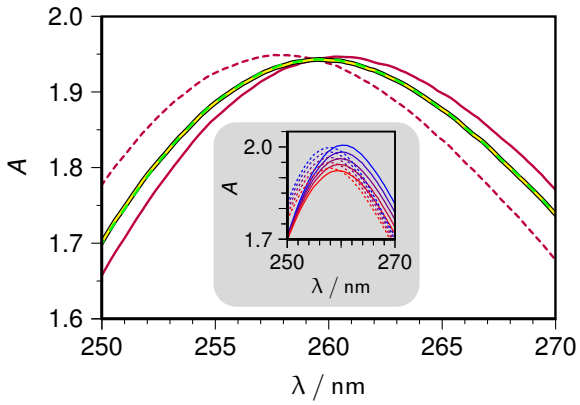

Supplementary Figure 2: Absorption spectra of 0.1 mM aqueous MV^{2+} plus additives; dashed monocoloured curves, with 0.1 mM S12S and 450 mM NaCl, and thus not associated with micelles ("aq"); solid monocoloured curves, in 50 mM SDS and without NaCl, and thus completely micelle-bound ("mic"). Main plot: measurements at 50 °C; yellow-green dashed curve with black borders, linear combination $0.65\,\mathrm{aq} + 0.35\,\mathrm{mic}$ superimposed on the experimental spectrum in 50 mM SDS and 450 mM NaCl, i.e., with partly micelle-bound Q. Inset: Absorption spectra of free and completely micelle-bound MV^{2+} at 20 °C (blue), 30 °C, 40 °C, 50 °C, and 60 °C (red); colours for the intermediate temperatures by linear interpolation. For further explanation, see the text.

By employing a weight-in concentration of MV^{2+} of 0.1 mM, we kept $\left[MV^{2+}_t\right]$ within the range used for our luminescence experiments. The corresponding optical densities at maximum lie slightly below 2; but, according to the manufacturer's specifications, our absorption spectrometer yields undistorted readings for extinctions up to 4; hence, a

sufficient resolution for spectral decomposition is ensured. We scanned the [NaCl]–T parameter space to incorporate all the grid points pertinent to the main article (0, 50, 150, 250, and 450 mM NaCl; 10, 20, 30, 40, 50, and 60 °C). However, insolubilities below 30 °C for the two highest NaCl concentrations restricted the combinations accordingly.

For the spectra of MV^{2+} in the aqueous bulk, we added an equimolar concentration of S12S (0.1 mM, i.e., well below the cmc) to take into account possible ion pairing. We found the wavelength of the absorption maximum (at about 258 nm) to be almost uninfluenced by the salt concentration. Completely micelle-bound MV^{2+} absorbs slightly red-shifted (by 2–3 nm), as already described in the literature.[6] With increasing temperature, both peaks move by minute amounts (1 nm over the investigated range) to the blue, and their maximum heights decrease marginally (by about 3 %). These changes, at the highest NaCl concentration, are visualized in the inset of Supplementary Figure 2.

As the main plot demonstrates, the MV^{2+} spectra in the presence of both S12S (above the cmc) and NaCl are perfectly represented by linear combinations of the aqueous and the micelle-bound spectra at the same T; and the coefficients are the ratios $\left[Q_{aq}\right] / [Q_t]$ and $[Q_m] / [Q_t]$, which we require for analyzing the luminescence decays. The dependence of the former ratio on NaCl content and temperature is displayed as the upper inset of Figure 2a of the main article.

3.2 Exit rates of MV^{2+}

The association equilibrium between MV^{2+}_{aq} in the aqueous phase and an S12S micelle to give micelle-bound MV^{2+}_{m} is formulated in Supplementary Equation S10,

$$MV^{2+}_{aq} + S12S_m \quad \underset{k_{diss}}{\overset{k_{ass}}{\rightleftharpoons}} \quad MV^{2+}_{m} \tag{S10}$$

This crude relationship neglects the possibility that a micelle hosts more than one molecule of MV^{2+} but suffices for obtaining an estimate.

The rate constant k_{ass} can be equated with the rate constant k_{ext} of quenching across the micelle–water interface because the rapid intramicellar quenching makes the attachment of an MV^{2+} molecule to the micelle the rate-determining step. Inserting this into the mass-action law and rearranging, one finally gets Supplementary Equation S11,

$$k_{diss} \quad = \quad k_{ext} \times \frac{[S12S_m]}{N_{agg}} \times \frac{[MV^{2+}_{aq}]}{[MV^{2+}_{m}]} \quad \leq \quad k_{ext} \times \frac{[S12S_t]}{N_{agg}} \times \frac{r}{1-r} \tag{S11}$$

To obtain the final expression, we have used Supplementary Equation S6 and also inserted the weight-in concentration of the surfactant $[S12S_t]$ instead of the smaller concentration $[S12S_m]$ in the aggregated state, which is conveniently available and provides an upper limit.

As seen in Figure 2a of the main article, k_{ext} is $2...4 \times 10^{10}\,M^{-1}s^{-1}$, and the ratio r is 0.7 or smaller, depending on the temperature and the NaCl content. With $[S12S_t]$ from

Supplementary Table 2 and N_{agg} from the fit functions of Supplementary Table 3, one thus arives at values of k_{diss} not exceeding $10^7\ s^{-1}$ in the worst case. There, however, the intramicellar quenching is completed within some 10 ns. More typical are values of k_{diss} of a few times $10^6\ s^{-1}$, and an intramicellar quenching regime of about 30 ns (see, the inset of Supplementary Figure 1b). Hence, the exit from the micelles is significantly slower than the intramicellar process.

3.3 Micellar Parameters Pertinent to Experiment Design and Analysis

The calculations of this Section presuppose that the micellar parameters do not respond to the addition of the small concentrations of Q, which lie below 1 mM throughout.

To this end, and to keep conditions similar between experiments on the different surfactants, we chose the weight-in concentrations [$Surf_t$] (denoted as c_t in Supplementary Table 2 and the further calculations to improve the readability) of the sodium alkyl sulfates S*n*S such that the concentration [$Surf_m$] of S*n*S present in aggregated form (as calculated with Supplementary Equation S13) was always 40–50 mM. Given that the maximum aggregation numbers N_{agg} are about 100 and the pyrene concentration was 10 μM, this also ensured a negligible probability of micelles hosting more than one fluorophore molecule.

Supplementary Table 2: Parameters pertinent to the measurements on sodium alkyl sulfates S*n*S with chain length *n*, and to their evaluation.

S*n*S	c_t[a] / mM	T_K[b] / °C	$cmc_0(T_0)$[c] / mM	T_0[c] / °C	σ[c]	α[d]	γ[e]
S9S	105	< 5 (2)	63.5	30.0	33.1	0.41	0.25
S10S	75	< 5 (2)	32.6	30.0	30.4	0.35	0.20
S11S	60	7	16.0	25.0	33.1	0.30	0.18
S12S	50	8–16 (13)	8.2	25.0	37.0	0.28	0.17[f]
S13S	50	21	4.2	22.5	37.3	0.22	0.26
S14S	45	20–30 (26)	2.0	20.0	39.1	0.19	0.20

[a] Weight-in concentration [$Surf_t$]. [b] Krafft temperature taken from Ref. 7; values in parentheses used for the calculations of $N_{agg,0}$ in the inset of Figure 3 of the main article. [c] Parameters for Supplementary Equation S12, values taken from Refs. 8–10. [d] Degree of micelle ionization, values taken from Ref. 9. [e] Exponent for Supplementary Equations S15–S17, values taken from Ref. 9. [f] This work, from the fit in Figure 3b of the main article.

Below the pertaining Krafft temperatures T_K, which are also contained in Supplementary Table 2, the solubility of each surfactant decreases drastically. This precluded measurements on S13S and S14S below 30 °C, and extrapolation had to be used to estimate N_{agg} in this range. Insolubilities also restricted the experimentally accessible temperature range when higher concentrations of NaCl were added to S12S: the lower limits were 20 °C with 150 mM, and 30 °C with 250 mM and 450 mM.

Supplementary Equation S13 below and the formulas of Section 3.4 are based on the cmc

without additives, denoted as cmc_0. In general, cmc_0 of sodium alkyl sulfates SnS exhibits a comparatively small temperature dependence, with a minimum near room temperature (cmc_0 at T_0), and is described by Supplementary Equation S12,[11]

$$\mathrm{cmc}_0(T) = \mathrm{cmc}_0(T_0) \exp\left[-\sigma\left(1 - \frac{T_0}{T} + \ln\frac{T_0}{T}\right)\right] \tag{S12}$$

where σ is a surfactant-specific constant. The parameters $\mathrm{cmc}_0(T_0)$, T_0, and σ necessary for obtaining $\mathrm{cmc}_0(T)$ under all our experimental conditions have been compiled in Supplementary Table 2.

The concentration of surfactant in the aggregated state $[\mathrm{Surf}_\mathrm{m}]$ can be calculated by a numerical solution of Supplementary Equation S13,[9,12] which involves the total concentration of sodium ions in the aqueous phase $\left[\mathrm{Na}^+_\mathrm{aq}\right]$,

$$\begin{aligned}\frac{c_\mathrm{t} - [\mathrm{Surf}_\mathrm{m}]}{\mathrm{cmc}_0(T)} &= \left(\frac{\left[\mathrm{Na}^+_\mathrm{aq}\right]}{\left(1 - V'_\mathrm{m} c_\mathrm{t}\right)\mathrm{cmc}_0(T)}\right)^{\alpha-1} \\ &= \left(\frac{c_\mathrm{t} + c_\mathrm{add} - (1-\alpha)[\mathrm{Surf}_\mathrm{m}]}{\left(1 - V'_\mathrm{m} c_\mathrm{t}\right)\mathrm{cmc}_0(T)}\right)^{\alpha-1}\end{aligned} \tag{S13}$$

where c_t and the concentration c_add of added NaCl are precisely known weight-in concentrations, V'_m the equally known molar volume of the anhydrous surfactant, $\mathrm{cmc}_0(T)$ follows from Supplementary Equation S12, and the degree of micelle dissociation of the micelle α is taken from Supplementary Table 2. A sufficiently accurate approximation of V'_m for SnS is given by Supplementary Equation S14,

$$\frac{V'_\mathrm{m}}{\mathrm{M}^{-1}} = 0.12 + 0.014n \tag{S14}$$

and amounts to a very minor correction only under our conditions.

Somewhat surprisingly, experimental results indicate α to be dependent neither on T nor on c_add;[9,13] hence, $\mathrm{cmc}_0(T)$ is the only variable that changes when a series of experiments as in Supplementary Figure 1a is repeated at a different temperature.

3.4 Micellar Aggregation Numbers

Our experimental results on the temperature dependence of the aggregation numbers $N_\mathrm{agg}(T)$ are very well represented by linear relationships in the temperature interval considered. Supplementary Table 3 lists the fit functions. Their quality can be judged by comparing them with the data points in Figures 3 and 3b of the main article; and by the standard deviations between the data and the fits, which are one unit.

For sodium alkyl sulfates at given temperature, an empirical relationship (Supplementary

Supplementary Table 3: Measured temperature dependence of the aggregation number N_{agg} of sodium alkyl sulfates SnS of chain length n (for S12S also with NaCl added).

SnS	[NaCl] / mM	best-fit $N_{agg}(T$ in K)
S9S	0	$144.0 - 0.3526T$
S10S	0	$176.1 - 0.4339T$
S11S	0	$222.8 - 0.5488T$
S12S	0	$234.8 - 0.5443T$
S12S	50	$313.4 - 0.7587T$
S12S	150	$362.9 - 0.8675T$
S12S	250	$392.0 - 0.9339T$
S12S	450	$464.6 - 1.1346T$
S13S	0	$338.3 - 0.7803T$
S14S	0	$343.9 - 0.7673T$

Equation S15) exists[13,14]

$$N_{agg} = \kappa_2 \left[Na^+_{aq}\right]^{\gamma} \tag{S15}$$

where $\left[Na^+_{aq}\right]$ again is the total concentration of sodium ions in the aqueous phase. Both κ_2 and γ are surfactant-specific.[9,13] No temperature-dependent investigations of Supplementary Equation S15 have been reported, but our observations (Table 3) that N_{agg} always is a linear function of T points to a linear temperature dependence of κ_2 and temperature independence of γ. This hypothesis is sustained by Figure 3b of the main article, where a fit with the same global γ successfully reproduces all the temperature-dependent data at different [NaCl].

Eliminating κ_2 with $N_{agg,0}$, which is the value of N_{agg} without additives and at a weight-in concentration equal to $cmc_0(T)$ leads to Supplementary Equation S16,

$$N_{agg} = N_{agg,0} \left(\frac{\left[Na^+_{aq}\right]}{cmc_0(T)} \right)^{\gamma} \tag{S16}$$

The term in parentheses on the right-hand side of Supplementary Equation S16 equals the one at the same position in Supplementary Equation S13. Rearanging and explicitly specifying all dependencies one arrives at Supplementary Equation S17,

$$N_{agg,0}\,(n, T) = N_{agg,exp} \left(\frac{c_t - [Surf_m]\,(n, T, c_t, c_{add})}{cmc_0\,(n, T)} \right)^{\frac{\gamma(n)}{1-\alpha(n)}} \tag{S17}$$

where the fraction enclosed by parentheses in Supplementary Equation S17 follows from the numerical solution of Supplementary Equation S13 and is, therefore, already available at this stage of the analysis. We stress that the apparent absence of the NaCl concentration from Supplementary Equation S17 is due to the fact that it is implicitly contained in $[\mathrm{Surf}_m]$.

3.5 Molar Volume of the Micelles

Direct measurements of the molar micellar volume V_m only seem available for S12S.[15] As an alternative, V_m can be calculated from N_{agg} with Supplementary Equation S18, which requires the knowledge of the partial molar volume in the aggregated state Φ_m.

$$V_m = \Phi_m N_{agg} \tag{S18}$$

Again, studies of Φ_m are very scarce. The only instances comprise a series of even-numbered alkyl sulfates at room temperature[16] and a limited temperature dependence for S12S.[17] Their results, as far as pertinent to this work, are displayed in Supplementary Figure 3.

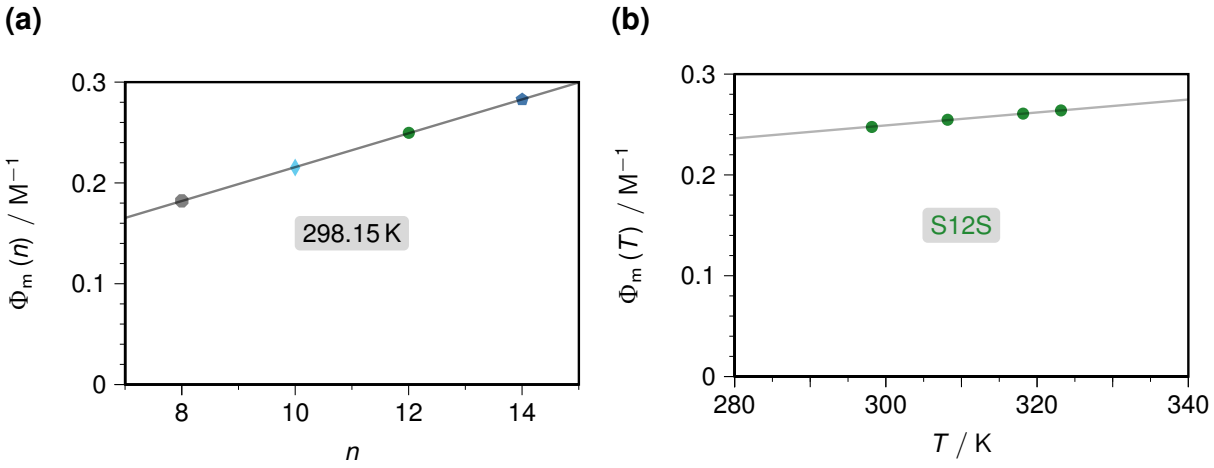

Supplementary Figure 3: Literature data for the partial molar volumes Φ_m of alkyl sulfates, with the global linear best fit by Supplementary Equation S19 given as straight lines. Graph (a), dependences on the length n of the alkyl chain;[16] graph (b), temperature dependence for S12S.[17] For further explanation, see the text.

Good local linear fits are found for Φ_m both as function of the number n of carbon atoms at constant temperature T (Supplementary Figure3a) and as function of T at constant n (Supplementary Figure3b). Both fits can be combined to give the global fit of Supplementary Equation S19,

$$\Phi_m = -0.129 + 0.0167n + 5.95 \times 10^{-4} T \tag{S19}$$

which is seen to reproduce all the existing data very well. The grid points of $\Phi_m(n)$ enclose all values of n used in our study, hence the interpolation for the odd-numbered chain lengths can be regarded as reliable. In contrast, a dependence of the temperature coefficient of Φ_m

on the chain length n cannot be excluded *per se*. However, for S12S the changes of Φ_m only amount to $\pm 7\,\%$ over the whole range of Supplementary Figure 3b, that is, the range relevant for the experiments herein. Because the differences between the temperature coefficients for different n are expected to be smaller than the coefficient at fixed n itself, the temperature coefficient of S12S seems a reasonable approximation for all the other surfactants as well, which is implicit in Supplementary Equation S19.

Combining this fit for Φ_m with the fits for $N_{agg}(T)$ compiled in Supplementary Table 3 yields the functions of Supplementary Table 4, which form provide the basis for the unified analyses of the quenching parameters in Figure 4 of the main article.

Supplementary Table 4: Molar volume of sodium alkyl sulfates SnS of chain length n (for S12S also with NaCl added).

SnS	[NaCl] / mM	Fit function (T in K)
S9S	0	$3.07 + 7.82 \times 10^{-2} T - 2.10 \times 10^{-4} T^2$
S10S	0	$6.69 + 8.83 \times 10^{-2} T - 2.58 \times 10^{-4} T^2$
S11S	0	$12.2 + 1.03 \times 10^{-1} T - 3.27 \times 10^{-4} T^2$
S12S	0	$16.8 + 1.01 \times 10^{-1} T - 3.24 \times 10^{-4} T^2$
S12S	50	$22.4 + 1.32 \times 10^{-1} T - 4.51 \times 10^{-4} T^2$
S12S	150	$25.9 + 1.54 \times 10^{-1} T - 5.16 \times 10^{-4} T^2$
S12S	250	$28.0 + 1.67 \times 10^{-1} T - 5.56 \times 10^{-4} T^2$
S12S	450	$33.2 + 1.95 \times 10^{-1} T - 6.75 \times 10^{-4} T^2$
S13S	0	$29.8 + 1.33 \times 10^{-1} T - 4.64 \times 10^{-4} T^2$
S14S	0	$36.0 + 1.24 \times 10^{-1} T - 4.57 \times 10^{-4} T^2$

Supplementary References

[1] T. Kohlmann and M. Goez, *Photochem. Photobiol. Sci.*, 2020, **19**, 71–79.

[2] M. H. Gehlen and F. C. De Schryver, *J. Phys. Chem.*, 1993, **97**, 11242–11248.

[3] P. P. Infelta, M. Grätzel and J. K. Thomas, *J. Phys. Chem.*, 1974, **78**, 190–195.

[4] M. Tachiya, *Chem. Phys. Lett.*, 1975, **33**, 289–292.

[5] *NIST Handbook of Mathematical Functions*, ed. F. W. J. Olver, Cambridge University Press, New York, 2010.

[6] H. J. D. McManus, Y. S. Kang and L. Kevan, *J. Phys. Chem.*, 1992, **96**, 2274–2277.

[7] N. M. van Os, J. R. Haak and L. A. M. Rupert, *Physico-chemical properties of selected anionic, cationic and nonionic surfactants*, Elsevier, 1993, pp. 9–40.

[8] P. Mukerjee and K. J. Mysels, *Stand. Ref. Data Ser., Nat. Bur. Stand. (US)*, 1971, **36**, 1–222.

[9] N. V. Lebedeva, A. Shahine and B. L. Bales, *J. Phys. Chem. B*, 2005, **109**, 19806–19816.

[10] I. Varga, R. Mészáros and T. Gilányi, *J. Phys. Chem. B*, 2007, **111**, 7160–7168.

[11] N. Muller, *Langmuir*, 1993, **9**, 96–100.

[12] F. H. Quina, P. M. Nassar, J. B. S. Bonilha and B. L. Bales, *J. Phys. Chem.*, 1995, **99**, 17028–17031.

[13] R. Ranganathan, L. Tran and B. L. Bales, *J. Phys. Chem. B*, 2000, **104**, 2260–2264.

[14] H. F. Huisman, *Proc. Kon. Ned. Akad. Wetensch.*, 1964, **B67**, 407–424.

[15] B. Hammouda, *J. Res. Natl. Inst. Stand. Technol.*, 2013, **118**, 151–167.

[16] S. Vass, T. Torok, G. Jakli and E. Berecz, *J. Phys. Chem.*, 1989, **93**, 6553–6559.

[17] A. Bhattarai, S. K. Chatterjee, T. K. Deo and T. P. Niraula, *J. Chem. Eng. Data*, 2011, **56**, 3400–3405.